

Water Surface Patch Classification Using Mixture Augmentation for River Scum Index

Takato Yasuno¹[0000-0002-4796-518X], Masahiro Okano¹, Sanae Goto¹,
Junichiro Fujii¹, and Masazumi Amakata¹

Yachiyo Engineering, Co.,Ltd. 5-20-8 Asakusabashi, Koto-ku, Tokyo, Japan
tk-yasuno@yachiyo-eng.co.jp

Abstract. Urban rivers provide a water environment that influences residential living. River surface monitoring has become crucial for making decisions about where to prioritize cleaning and when to automatically start the cleaning treatment. We focus on the organic mud, or "scum" that accumulates on the river's surface and gives it its peculiar odor and external economic effects on the landscape. Because of its feature of a sparsely distributed and unstable pattern of organic shape, automating the monitoring has proved difficult. We propose a patch classification pipeline to detect scum features on the river surface using mixture image augmentation to increase the diversity between the scum floating on the river and the entangled background on the river surface reflected by nearby structures like buildings, bridges, poles, and barriers. Furthermore, we propose a scum index covered on rivers to help monitor worse grade online, collecting floating scum and deciding on chemical treatment policies. Finally, we show how to use our method on a time series dataset with frames every ten minutes recording river scum events over several days. We discuss the value of our pipeline and its experimental findings.

Keywords: water environment, river surface, scum detection, image augmentation, scaled heatmap index

1 Introduction

1.1 Related Works

The automated garbage collector and river cleaning robot have been the center of the river manager assisted robotics research for the past decade [1,2]. Additionally, the river surface monitoring has become crucial to decide which areas are the worst and to automatically begin the cleaning process. Since 1991, there have been numerous studies for understanding the scum formation mechanism in-house experiments [3,4], field observations regarding organic sludge and odor [5,6], and automatic scum behavior monitoring using river surface computer vision [7][8]. Owing to the complex events and intertwined phenomena that include physical, chemical, biological, and hydrological features, it is not widely known how to fundamentally solve the river scum problem.

After a few days of rainfall, combined sewer overflows (CSOs) have suddenly occurred at the upstream of the river owing to scum and the highly dispersed residential living environment. The river’s odor and external economic effects on the landscape are then caused by organic mud, or ”scum” that appears on the river’s surface. Mizuta et al. [8] proposed a method for monitoring scum in urban river’s tidal area. The 805 split lattice color images with a 20×20 pixel size were automatically used by the fixed point camera to determine whether or not scum was present. The accuracy to identify the scum ranged from 58 to 88 percent using this straightforward neural network model with one hidden layer. The input variables include the 45 features of statistics and 25, 50, and 75 percentiles for each pixel’s RGB components. Additionally, they included input features like bridges and fences as reflected background features that were visible on the water surface. Although this was a preliminary version of the scum monitoring method, there is still room for accuracy enhancement and generalization to deep learning algorithms for pixel-by-pixel classification, also known as semantic segmentation, such as the U-Net [9]. Nakatani et al. [10] studied detailed observations of scum using multiple cameras and sediment surveys in a tidal river to understand the generation and floating behavior of scum using the U-Net. They discovered evidence that the local flow may have a significant impact on the spatial-temporal behavior of the scum owing to the tide level. Semantic segmentation is unquestionably a possible option for a roughly scum monitoring method. If we use the marine debris object type [11,12], which includes bottle, can, hook, and tire, the U-Net with the ResNet34 backbone was still the best performing model. However, it has not always high accuracy with a value of Intersection of Union 0.748.

However, the scum feature has sparsely distributed and unstable pattern, making it difficult to improve the semantic segmentation accuracy. The scum segmentation on the river surface still has an over-prediction issue, and it is insufficiently accurate for scum monitoring on the river water surface. The area of interest, the scum, was obscured by the water surface, which was frequently reflected by the nearby background features such as building, bridge, pole, sign, sky, and trees. The authors propose a patch-wise classification method using image augmentation to improve the precise recognition of the river scum.

1.2 Pixel-wise Segmentation vs Patch Classification

First, we debate whether supervised learning such as used in classification, object detection, and semantic segmentation, is a better deep learning approach. We can select the semantic segmentation or classification if the target feature of the scum is not categorized into object context. It becomes challenging to annotate the scum feature on the pixel-wise region of interest (ROI) within the river surface in the case of the semantic segmentation. The scum features are sparsely dispersed, and the pattern is unstable and complex. The training results would be low precision and the false negative error, which predict scum but actually background, would increase if we attempted to annotate one of the filled regions with multiple scum features. Therefore, the authors proposed a

patch-wise classification approach rather than the pixel-wise semantic segmentation. The patch size is 128×256 . In contrast, we can consider an approach from unsupervised learning like the generator and anomaly detection such as the Variational Auto-Encoder (VAE) [13].

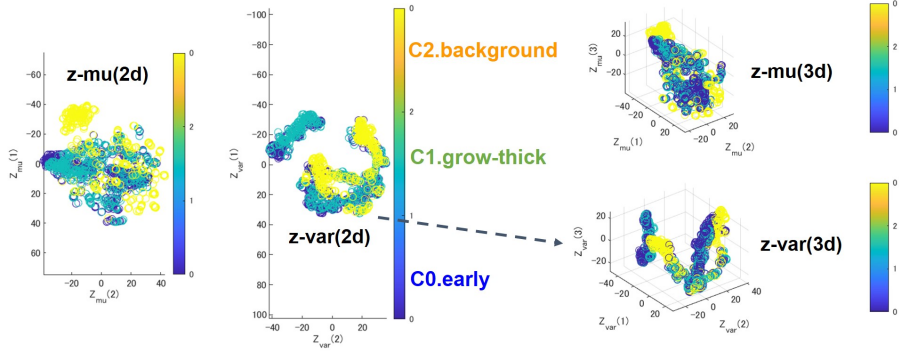


Fig. 1. Scum Feature of z-space Trained from 3 classes Conditional VAE (defined by C0:early scum, C1:grow-thick scum, C2:background. Training dataset has respectively (5,026, 4,070, 4,308). Test dataset has each classes (550, 450, 470).)

As illustrated in **Fig.1**, we demonstrated how to train the three classes of conditional VAE [14] using a dataset that was defined by C0. "early scum," C1. "grow-thick scum," and "background." Here, the bridge z-space contains 256 elements. Using t-SNE, we could dimension-reduce the z-mean and z-variance into plots of two and three dimensions. Hence, the three classes of river water surface, scum-generated feature, and a background that includes the building, train, bridge, barrier, pole, and tree, were not independent of each other. Here, a fake scene was reflected on the river's water surface with a mirrored background rather than an actual image. Thus, river water surface images are very complex and dependent on the water surface class and the target scum feature. Therefore, we will not select the generative learning and pixel-wise segmentation approaches. We discovered that it is not fitted to the dataset of river scum images for accurate scum detection. To tackle the low precision problem, this study proposed a patch-wise classification approach using mixture image augmentation.

1.3 Objective and Pipeline

As shown in **Fig.2**, we give an overview of the pipeline from the offline training stage to the online prediction and computing scum index. The first three components of the training stage are 1) data preparedness, 2) mixture image

augmentation, 3) patch classification deep learning. The data preparation process involves cropping a rectangle without the far region's top and extracting four rows by five columns of patch images. Mixture image augmentation [15] transforms into diversified images using multiple raw images, such as the mixup [16,17], Cutout [18], and RICAP [19]. A convolutional neural network, such as the ResNet50, is used in deep learning for patch classification. Secondly, the prediction stage using the pre-trained deep network includes the following steps: 1) predict 20 patch probabilities; 2) combine their probabilities into a matrix; 3) create a scaled heatmap; 4) binarize the mask image; and 5) calculate the pixel count of the scum region. The prediction brings the total number of patch probabilities taken from the raw input frame to 20. Their probability values are combined into a matrix. The matrix with four rows by five columns is transformed into a scaled heatmap with a grayscale intensity range of 0 to 255. The heatmap can binarize a mask image with pixels set to 0 or 1. The scum region pixel with a value of one on the mask image can be counted. Finally, the temporal scum index at a time stamp is computed as the value we call "scum-on-river" ratio whose scum region pixel count is divided by the river region pixel count, ranging from 0 to 100 percent. Here, the river region can count pixels without a background. The background region is constant when the camera angle is fixed, allowing us to set the river region's pixel count. We can repeatedly calculate the scum-on-river ratio using the raw input frame image collected every ten minutes. We can visualize the time series of scum-on-river ratio and draw the color heatmap ranging from blue to red.

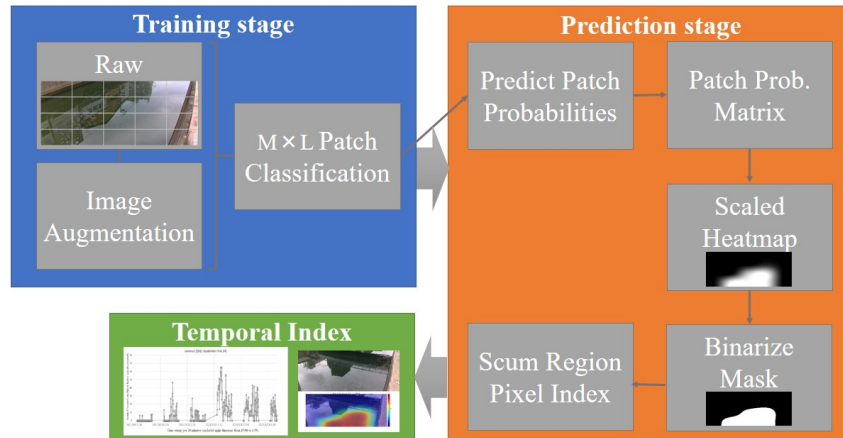


Fig. 2. Pipeline Overview from A Camera Frame Input to "scum-on-river" Ratio

To distinguish between the floating scum feature and the entangled background on the river surface mirrored close to structures like buildings, bridges, poles, and barriers, we propose a patch classification pipeline to detect scum regions on the river surface using mixture augmentation. We also proposed a "scum-on-river" ratio index to help with online scum appearance degradation and decision-making regarding collecting floating scum and chemical treatment policy. Finally, we demonstrated how to use our pipeline on a time series of frames every ten minutes, recording the river scum vision for several days at an urban river in Japan 2021.

2 Water Surface Detection Method

2.1 Crop Far Region and Patch Classification

The first three steps of the training stage are data preparation, mixture image augmentation, and deep learning patch classification. The data preparation operates to crop a rectangle without the top of the far region and to extract four rows by five columns of patch images, as illustrated in **Fig.3**. The size of the river vision camera used in this study is 1,280 pixels wide by 720 pixels high. We precisely cut the top of the rectangle at 1,280 pixels in width and 108 pixels in height, because this relatively remote area has extremely low resolution and the background noise from the bridge, building, pole and barrier. The remaining image is therefore 128×256 in size and 512 by a width 1,280 ; hence, we can extract it based on a patch image. We can thus create a patch image with four rows by five columns. We define the scum condition on the river surface: C0: early scum, C1: grow-thick scum, and C2: background. Convolutional neural networks (CNNs) can be used to implement deep learning to classify patch images into 3 classes as a supervised learning e.g. the ResNet18, ResNet50 [20], MobileNetv2 [21] and self-supervised and unsupervised learning [22]. We chose the ResNet50 as the default CNN of supervised classification model; this deep network is frequently used to facilitate transfer learning.



Fig. 3. Example of Patch Images Cropped Upper Far Region

2.2 Image Augmentation for Variety and Disentanglement

The past decade has seen renewed importance of augmented image data for deep learning [13]. Image data augmentation is categorized into two i.e., basic image manipulation and deep learning approaches. The former augmentation includes 1) kernel filters, 2) geometric transformations, 3) random erasing, 4) mixing images, and 5) color space transformations. The latter consists of three components: 1) adversarial training, 2) neural style transfer, and 3) GAN model-based transformation. Particularly, geometric transformation, image blending, and neural style transfer have contributed to meta learning [15]. The deep learning-based augmentation could not be fitted to the target dataset of the river surface because of the features entangled between the region of interest in the scum and the background mirroring the building, bridge, pole and barrier. This study proposes the fundamental image manipulations, such as mixing and random erasing of images. To detangle the river surface feature, the random erasing technique is straightforward and efficient as the regional dropout in the training images. We also believe that the augmentation of mixing images diversifies the river water surface feature. Using multiple raw images, the mixture image augmentation creates diversified images, like the mixup [16,17], Cutout [18], and RICAP [19]. Convolutional neural network deep learning is used for a patch classification.

As illustrated in **Fig.4**, the mixup is a linear combination manipulation using two randomly sampled images X_i, X_j . Here, we set the random weight parameter $\lambda \in [0, 1]$. This weight parameter is randomly generated from the Beta distribution $Beta(\alpha, \alpha)$ where it takes a value between $[0, 1]$. It is generated from the uniform distribution when $\alpha = 1.0$. When $\alpha = 0.2, 0.4$, the peakiness on both sides increases in a bustab-like shape. Therefore, we can write the following two equations to represent the mix-up image augmentation.

$$\tilde{M} = \lambda X_i + (1 - \lambda) X_j \quad (1)$$

$$\tilde{C}_{mixup} = \lambda z_i + (1 - \lambda) z_j \quad (2)$$

Here, two randomly selected images from different classes are labeled z_i, z_j , and the augmented new label \tilde{C}_{mixup} results in one-hot encoding. Notably, the mixup augmentation never enhances the overall performance of classification deep learning, even if two images were randomly selected from the same class.

As shown in **Fig.5**, the Cutout is a straightforward regularization technique that involves random masking out square input regions during training. Inspired by the dropout regularization mechanisms, this is an extremely easy implementation, but it could be combined with the existing form of data augmentation to further enhance model performance. To apply to situations like occlusion, the Cutout image augmentation has been labeled "regional dropout". This regional dropout has been used with the drop rate $d \in \{0.3, 0.4, 0.5, 0.6\}$ in the past experimental studies on natural image recognition datasets. The complex entangled features on the river surface could be disentangled using the Cutout regularization. The entangled features included the scum floating organ and mirrored sky, bridge, building, and pole backgrounds.



Fig. 4. The mixup Augmented Images of Scum grow-thick class



Fig. 5. The Cutout Augmented Images of Scum grow-thick class

As illustrated in **Fig.6**, the random image cropping and patching (RICAP) technique involves mixing four randomly cropped images, respectively, and concatenating them into a new augmented image. The RICAP greatly expands the variety of images and prevents overfitting of deep convolutional neural networks. Image data manipulation is done in three steps. First, we can randomly select four images $m \in 1, 2, 3, 4$ from the practice dataset. On the upper left ($m = 1$), upper right ($m = 2$), lower left ($m = 3$), and lower right sides ($m = 4$), we patch them in that order. Second, we can crop the images separately. \bar{w} and \bar{h} denotes the width and height of the training image, respectively. We can randomly set the boundary position (w, h) of the four images m from a uniform distribution. This is known as the variant *anywhere*-RICAP.

$$w \sim U(0, \bar{w}), h \sim U(0, \bar{h}) \quad (3)$$

Then we can automatically obtain the cropping sizes (w_m, h_m) of the image m . i.e., $w_1 = w_3 = w$, $w_2 = w_4 = \bar{w} - w$, $h_1 = h_2 = h$, and $h_3 = h_4 = \bar{h} - h$. For cropping the four images m following the sizes (w_m, h_m) , we can randomly

determine the coordinates (x_m, y_m) of the upper left corners of the cropped areas as $x_m \sim U(0, \bar{w} - w_m)$ and $u_m \sim U(0, \bar{h} - h_m)$. Thirdly, we can patch the cropped images to construct a new image. We can mix the four images' class labels with ratios proportional to the areas of the cropped images. Therefore, using the following equation, we define the target label \tilde{C}_{RICAP} by mixing one-hot coded class labels c_m of the four patched images with ratios Λ_m proportional to their areas in the newly constructed image.

$$\tilde{C}_{RICAP} = \sum_{m \in \{1,2,3,4\}} \Lambda_m c_m \quad (4)$$

$$\Lambda_m = \frac{w_m h_m}{\bar{w} \bar{h}}, \quad (5)$$

where $w_m h_m$ is the area of the cropped image m and $\bar{w} \bar{h}$ is the area of the original image. Note that even if four images were randomly selected from the same class, the RICAP augmentation never improve the overall performance of classification.



Fig. 6. The RICAP Augmented Images of Scum grow-thick class (Random Image Cropping and Patching)

2.3 Scum-on-River Ratio Metrics

In the prediction stage using the pre-trained deep network, it includes the following steps: 1) predict 20 patch probabilities; 2) combine their probabilities into a matrix; 3) create a scaled heatmap; 4) binarize the mask image; and 5) pixel count of scum region. The prediction brings the total number of patch

probabilities extracted from the raw input frame to 20. Their probabilities' values are combined into a matrix. The matrix with four rows by five columns is transformed into a scaled heatmap with a grayscale intensity range of 0 to 255. The heatmap can binarize a mask image with pixels set to 0 or 1. The translated binary mask image and the gray scaled heatmap from patch probability matrix are shown together in **Fig.7**.

The scum region pixel whose value is one on the mask image can be counted. Finally, the temporal scum index at a time stamp is calculated as the value, we call "scum-on-river" ratio whose scum region pixel count is divided by the river region pixel count, ranging from 0 to 100 percent.

$$ratio = \frac{pixels(scum)}{pixels(I - background)} = \frac{pixels(scum)}{pixels(river)} \quad (6)$$

Here, I denotes the cropped raw input image without remote area of upper rectangle. The river region can count the pixels without background. When the camera angle is fixed, the background area remains constant, allowing us to set the river region's pixel count.

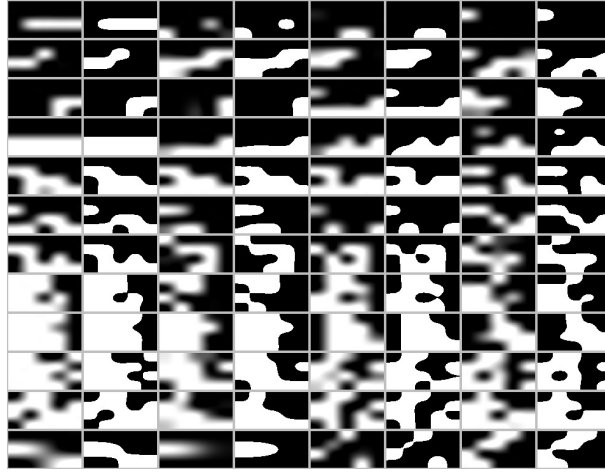


Fig. 7. Example of Binarized Mask Images from Patch Probability Scaled Heatmap

3 Applied Results

3.1 Frame Data Preparedness

River scum is a rare occurrence, and it is difficult to collect its appearance before it gets too thick. We prepared a time series dataset to focus on the weeks when

the scum first appeared, and we extracted frames per ten minutes from some recorded videos at an urban river around a densely populated area. A combined sewer station operates upstream of the city river. We show how to apply our method on two weekly time series with a frame every ten minutes, where river scum events have been occurring for several days.

3.2 Training Results and Test Accuracy

For training classification, used 884 frame images scum occurrence in 2021. The 13 cameras were continuously recording the scum conditions along an urban river and monitor the scum condition. We divided the training and test images in a 9:1 ratio. The image is $720 \times 1,280$ in both height and width. We have prepared 14,404 patches for the deep learning model’s training, and the 1,470 patches for evaluating test accuracy. We trained the ResNet50 using a baseline model and several image augmentations such as mixup, Cutout, and RICAP.

The test accuracy comparison of the patch classification and mixture image augmentation is shown in **Table 1.** Here, we define the three classes of river surface conditions, C0: early scum, C1: grow-thick scum, and C2: background. At the three-row level of the mixup augmentation, it never achieves a higher level of accuracy than the baseline ResNet50 model. The linear mixing strategy was inefficient to generalize performance. However, it outperformed the baseline model with test accuracy + 0.6 and on the precision + 1.7 when displaying the four rows of the Cutout augmentation. The highest score among ablation studies was achieved by the drop rate $d = 0.6$. However, the recall accuracy was the same as in the baseline model. The RICAP augmentation + 0.5 outperformed the recall accuracy than the baseline model. The RICAP has improved the test accuracy and the precision over the baseline model by + 0.3 and + 0.4, respectively. For scum detection and monitoring to decrease the scum-positive false error, where predict negative scum but actually scum, the recall accuracy is essential. Thus, we chose the ResNet50 + RICAP result, setting the pre-trained network to predict the patch probabilities and displaying the scum heatmap.

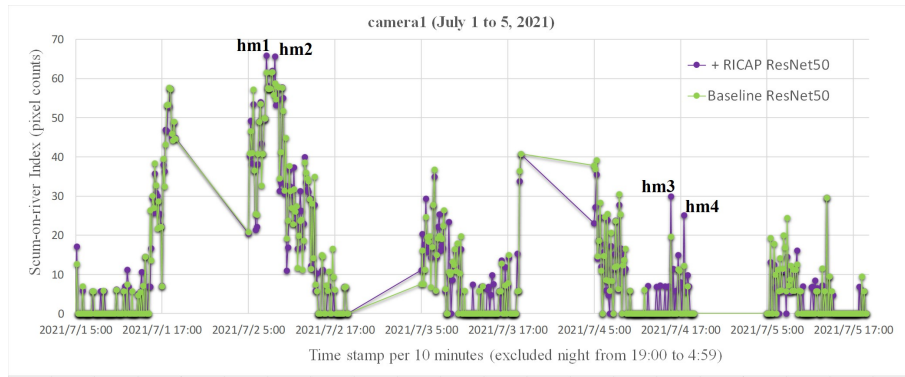
3.3 Visualize Heatmap and Temporal Scum Index

As shown in **Fig.8**, the left side of the two heatmaps could precisely detect the peak of scum appearance. This refers to the feasibility of using our proposed scum-on-river ratio index to monitor the grade of scum generation. In contrast, two heatmaps on the right have been over predicted to incorrectly attend the building background noise mirrored on the river surface. The waving on the river surface after a boat has passed is what causes scum-negative false errors.

As shown in **Fig.10**, we have depicted the camera’s scum-on-river ratio index, which is pixel-based measured along the vertical axis. In contrast, the horizontal axis indicates the average probability of each patch’s predicted value to predict the target class, i.e., C1: grow-thick scum of probabilities. This is a linear relationship between the probability matrix and the scum region pixels. Notably, the scum-on-river index’s limitation was set at more than five percent,

Table 1. Test Accuracy Comparison of Patch Classification and Mixture Image Augmentation (3 classes defined by early scum, grow-thick scum, and background)

Model	Augmentation	Test accuracy	Precision	Recall
ResNet50	Baseline	97.4	97.6	94.6
ResNet50	+ mixup($\alpha = 1.0$)	95.1	96.1	89.1
ResNet50	+ mixup($\alpha = 0.2$)	97.4	97.6	94.4
ResNet50	+ mixup($\alpha = 0.4$)	97.4	97.6	94.4
ResNet50	+ Cutout($d = 0.3$)	97.5	99.3	93.4
ResNet50	+ Cutout($d = 0.4$)	97.8	99.5	94.0
ResNet50	+ Cutout($d = 0.5$)	97.8	99.3	94.2
ResNet50	+ Cutout ($d = 0.6$)	98.0	99.3	94.6
ResNet50	+ RICAP	97.7	98.0	95.1

**Fig. 8.** Results of Temporal Scum-on-River Ratio Index (camera1)

resulting in an average probability set at more than 0.01. This explains why the extremely small average probability produced an incorrectly unstable heatmap. We set zero probability if the average probability of each patch prediction is less than or equal to 0.01.

As shown in **Fig.11**, on the left of heatmap "hm5," we identified the possibility of accurately detecting the night scum appearance as early as 5:20 am, regardless of a little dark situation. In contrast, the second heatmap "hm6" had made an incorrect prediction regarding the light rainfall noise reflected on the river surface. This explains why the scum feature from the AI view of the pre-trained classification network and the reflecting rainfall on rivers are similar. Because the training dataset of this work excluded the rainfall background to generalize the hydrologic context, two heatmaps "hm7" and "hm8" could initially recognize the scum appearance on the right. This indicates the feasibility

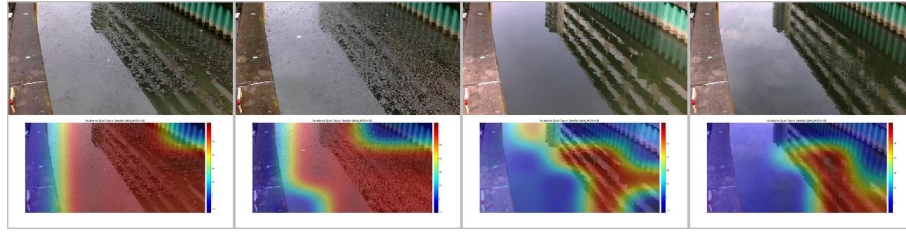


Fig. 9. Heatmap at Excess Ratio of Scum-on-River Index (camera1 shown in **Fig. 8** from the left of "hm1" to the right of "hm4" in order.)

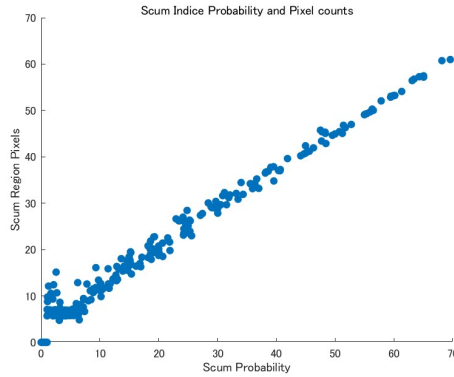


Fig. 10. Plot of Scum-on-River Ratio Index (camera1: Vertical axis is pixel based, Horizontal axis is probability based)

of monitoring the start of scum generation using the proposed scum-on-river ratio index.

As shown in **Fig. 13**, we drew the camera2’s scum-on-river ratio index, which is pixel-based computed by the vertical axis. Alternatively, the horizontal axis represents the average probability of each patch’s predicted value to predict the target class, i.e., C1: grow-thick scum of probabilities. The probability matrix and the scum region pixels in the scum region are also linear related. Similarly, note that the scum-on-river index’s upper limit is set at more than 5 percent, resulting in an average probability that is at or below 0.01. This explains why the extremely small average probability produced an anomalous heatmap owing to the negative value of the scaled heatmap. Therefore, if the average probability of each patch prediction is less than or equal 0.01, we set zero probability.

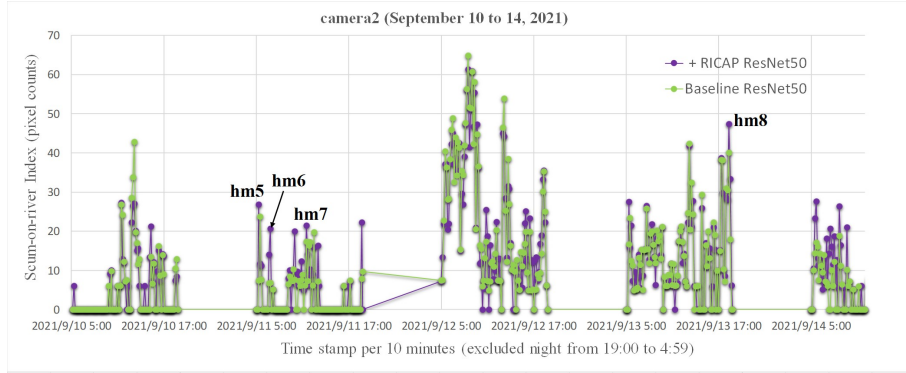


Fig. 11. Results of Temporal Scum-on-River Ratio Index (camera2)

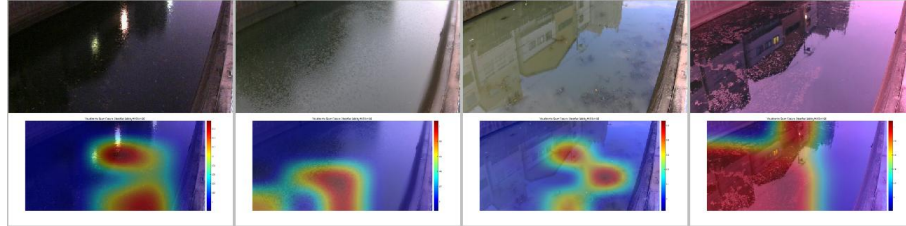


Fig. 12. Heatmap at Excess Ratio of Scum-on-River Index (camera2 shown in Fig.11 from the left of "hm5" to the right of "hm8" in order.)

4 Concluding Remark

4.1 Experimental Studies and Lessons

We suggested using image augmentation to increase the variety and disentangled regularization in a patch classification to identify scum features on river surfaces. We precisely trained the ResNet50 network’s baseline. We have enhanced river surface images using the mixup, Cutout, and RICAP for accuracy comparison. We found that the RICAP outperformed the baseline model and other augmentations in terms of recall accuracy, 95.1 percent and prediction 98.0 percent. We also discovered that the Cutout could improve the precision by 99.3 percent. Furthermore, we provided an assisted metric to make it possible to compute a scum-on-river ratio index for river scum monitoring and heatmap visualization. With the grow-thick scum class, we could set the average probability’s bottom line to 0.01, insignificant probability that prevented an unstable scale heatmap. Using this setting, we could illustrate a scum-on-river ratio of greater than five percent when we implemented experimental studies to our river surface dataset. Finally, we demonstrated how to use our pipeline to images from urban cam-

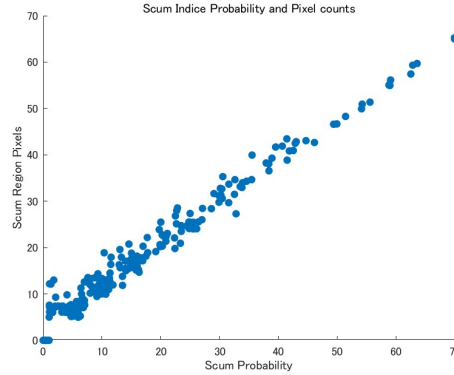


Fig. 13. Plot of Scum-on-River Ratio Index (camera2: Vertical axis is pixel based, Horizontal axis is probability based)

eras. The dataset of time series frames every ten minutes included scum growing events and thick conditions on two weeks, July, and September 2021 in Japan. We discovered that the limitation that background noise such as building reflections on the surface, and light rain waves on the river’s surface influenced the false positive error. We also discovered the feasibility of detecting the scum appearance in the early morning hours.

4.2 Future Works

The off-line training and prediction results are limited in this study. Several obstacles for on-line assisted river managers address the water surface vision problem. First, it reduces rain noise in relation to rain reflection on the river surface on rainy days. Second, we should monitor the river surface during the night, in the early morning five o’clock and after 19 o’clock because the scum growing event could have occurred at night. Third, it becomes crucial to forecast the scum excess time more than the water quality level. We can collect additional time series datasets such as temperature, rainfall, and river water level. Using these temporal variables, we can multi-mode learning to forecast the growing scum trend and the peak of scum index level. Fourth, the rare frequency of scum events makes the supervised training too much time and the data collecting cost. So we exploit the self-supervised and unsupervised approach to create more general pipeline. River water environment will still impact urban life around the world. We will attempt to automate river water vision monitoring that assists for water environment cleaning.

Acknowledgements We thank Takuji Fukumoto and Shinichi Kuramoto (Math-Works Japan) who contributed to support the MATLAB resources on Image Data Augmentation for Deep Learning.

- [1] O. Nurlansa, D.A. Istiqomah et al. 2014 : "AGATOR as Automatic Garbage Collector Robot Model", *International Journal of Future Computer and Communication*, Vol. 3, No. 5.
- [2] K.A. Ingle, A.G. Bhatkar et al. 2020 : "River Cleaning Robot Using Solar Power", *International Journal of Progressive Research in Science and Engineering* Volume-1, Issue-4.
- [3] M. Yamazaki, T. Tsukui 1991 : "Study on the Occurrence of Scum in River (Part2) Results of Sedimentation Survey in Kanda River Between Shiratori Bridge and Iida Bridge", *Annual Report of the Tokyo Metropolitan Research Institute for Environmental Protection*, 182-184.
- [4] M. Sugawara, M. Ishikawa et al. 1995 : "Formation Mechanism of Scum in Polluted Rivers", *Journal of Environmental Conservation Engineering*, Vol. 24, No. 7, 402-405.
- [5] S. Miura, T. Ishikawa et al. 2018 : "Field Observations on Accumulation of Organic Sludge and Generation of Scum in Nomi-River Flowing through Highly Urbanized Area of Tokyo", *Journal of JSCE, Ser. B1(Hydraulic Engineering)*, Vol. 74, No. 4, 523-528.
- [6] J.C. Casilia, R. Okuyama et al. 2019 : "Hydrodynamic Feature, Appearance of Scum, and Spatial Distribution of Odor in Urban Estuaries", *Journal of JSCE, Ser. G (Environmental Research)*, Vol. 75, No. 5, 141-146.
- [7] Y. Nakatani, Y. Iwaoka et al. 2022 : "Generation and Floating Behavior of Scum in An Urban Tidal River in Osaka, Japan", *Journal of JSCE* Vol.10, 228-234.
- [8] S. Mizuta, T. Takasaki et al. 2015 : "Automatic Distinction of Scum in Urban River by Neural Network Using Fixed Point Camera Image", *Journal of JSCE, Ser. B1(Hydraulic Engineering)* Vol.71, No.4, 1231-1236.
- [9] O. Ronneberger, P. Fischer et al. 2015 : "U-Net: Convolutional Networks for Biomedical Image Segmentation", *Proceedings of the 18th International Conference on Medical Image Computing and Computer-Assisted Intervention*, 234-241.
- [10] Y. Nakatani, M. Okumura et al. 2020 : "Continuous Observation Method of Floating Objects at River Surface Using U-Net", *Journal of JSCE, Ser. B1 (Hydraulic Engineering)*, Vol. 76, No. 2, 997-1002.
- [11] S. Deepak, V.-T. Matias 2021 : "The Marine Debris Dataset for Forward-Looking Sonar Semantic Segmentation", preprint arXiv:2108.06800v1.
- [12] H. Jungseok, F. Michael et al. 2020 : "A Semantically-segmented Dataset towards Visual Detection of Marine Debris", preprint arXiv:2007.08097.
- [13] D.P. Kingma, M. Welling 2013 : "Auto-Encoding Variational Bayes", preprint arXiv:1312.6114v10.
- [14] S. Kihyuk, H. Lee, and X. Yan 2015 : "Learning Structured Output Representation using Deep Conditional Generative Models", *Advances in Neural Information Processing Systems* 28, NIPS2015.
- [15] C. Shorten, T.M. Khoshgoftaar 2019 : "A Survey on Image Data Augmentation for Deep Learning", *Journal of Big Data*, 2019, 6:60.

- [16] H. Zhang, M. Cisse et al. 2017 : "Mixup: Beyond Empirical Risk Minimization," preprint arXiv:1710.09412.
- [17] K. Tango, T. Ohkawa et al. 2022 : "Background Mixup Data Augmentation for Hand and Object-in-Contact Detection", preprint arXiv:2202.13941v2.
- [18] T.D. Vries, G.W. Taylor 2017 : "Improved Regularization of Convolutional Neural Networks with Cutout", preprint arXiv:1708.04552v2.
- [19] R. Takahashi, T. Matsubara et al. 2018 : "RICAP: Random Image Cropping and Patching Data Augmentation for Deep CNNs", ACML2018, Proceedings of Machine Learning Research 95, 786-798.
- [20] K. He, X. Zhang et al. 2015 : "Deep Residual Learning for Image Recognition", preprint arXiv:1512.03385v1.
- [21] M. Sandler, A. Howard et al. 2018 : "MobileNetV2: Inverted Residuals and Linear Bottlenecks", The IEEE Conference on Computer Vision and Pattern Recognition (CVPR), 4510-4520.
- [22] L. Schmarje, M. Santarossa et al. 2021 : "A Survey on Semi-, Self- and Unsupervised Learning for Image Classification", IEEE Access 2021.